Endothelial Cell Electrical Impedance Parameter Artifacts Produced by a Gold Electrode and Phase Sensitive Detection

Anthony E. English*, James C. Squire, *Senior Member, IEEE*, James E. Bodmer, and Alan B. Moy

***Abstract*—Frequency dependent cellular micro-impedance estimates obtained from a gold two-electrode configuration using phase sensitive detection have become increasingly used to evaluate cellular barrier model parameters. The results of this study show that cellular barrier function parameter estimates optimized using measurements obtained from this biosensor are highly susceptible to both time dependent and systematic instrumental artifacts. Based on a power spectral analysis of experimentally measured microelectrode voltages, synchronous, 60 Hz, and white Gaussian noise were identified as the most significant time dependent instrumental artifacts. The reduction of these artifacts using digital filtering produced a corresponding reduction in the optimized model parameter fluctuations. Using a series of instrumental circuit models, this study also shows that electrode impedance voltage divider effects and circuit capacitances can produce systematic deviations in cellular barrier function parameter estimates. Although the implementation of an active current source reduced the voltage divider effects, artifacts produced by coaxial cable and other circuit capacitive elements at frequencies exceeding 1 kHz still remained. Reducing time dependent instrumental fluctuations and systematic errors produced a significant reduction in cellular model barrier parameter errors and improved the model fit to experimental data.**

***Index Terms*—Biological cells, biomedical transducers, impedance, measurement errors, parameter estimation.**

I. Introduction

IMPEDANCE measuements have become increasingly used to characterize and study biological cells. A novel cellular microimpedance measuring system pioneered by Giaver and Keese, [1]–[3], referred to as the electric cell substrate impedance sensor (ECIS), has found widespread application in toxicology screening, cellular motility, and cellular adhesion interaction studies [4]–[17]. Frequency dependent cellular impedance measurements obtained from this sensor can be used to estimate cellular barrier function parameters based on closed form solutions to a cellular impedance model [18]–[20]. Despite the potential importance of this biosensor, however, few studies have considered the sources of random and systematic instrumental artifacts in this system and their impact on cellular barrier function parameter estimates [21].

This biosensor is based on a gold two-electrode configuration where cells are cultivated on a small gold surface and subjected to ac currents on the order of 1 μA. Phase sensitive detection of the electrode voltage is used to estimate the cell monolayer impedance at specific reference frequencies knowing the applied current. During the phase sensitive detection process, however, several forms of random and deterministic electrical noise can corrupt the voltage signal. These artifacts, appearing at different frequencies and intensities depending on the sampling rate, filter time constant, and filter roll off, contribute to fluctuations in cellular barrier impedances and parameter estimates. The quantification of these random and deterministic noise sources is, therefore, necessary to distinguish between impedance and barrier parameter fluctuations that have a true physiologic meaning from those produced by instrumental artifacts.

The introduction of systematic errors produced by the voltage to impedance conversion in this system must also be carefully considered. In most studies of this nature, a large resistor is connected in series with the electrode and an ac voltage generator to produce a passive current source. Assuming that such a system produces a constant electrode current, however, ignores the voltage divider effects produced by the electrode impedance and capacitances associated with the coaxial cables and other circuit elements. These artifacts produce systematic shifts in the impedance and parameter estimates. This study, therefore, carefully examines both the time dependent and systematic errors that corrupt endothelial cell impedances and their propagation into cellular barrier function parameter estimates.

II. Methods and Materials

A. Cell Culture

Endothelial cells were isolated from porcine pulmonary arteries obtained from a local abattoir and cultivated in an incubator at 37 °C and 5% CO_2. The cell culture media consisted of M199 (GibcoBRL) and 10% fetal bovine serum (Hyclone) supplemented with vitamins (Sigma), glutamine (GibcoBRL), penicillin and streptomycin (GibcoBRL), and amino

Manuscript received August 13, 2005; revised October 21, 2006. The work of A. E. English was supported in part by the National Science Foundation under CAREER Award BES-0238905. The work of A. B. Moy was supported in part by the American heart Association under Grant 0265029B and in part by the National Institute of Health under Grant R016M61732.. *Asterisk indicates correspondng author.*

*A. E. English is with the University of Tennessee, Knoxville, TN 37996 USA (e-mail: tenglish@utk.edu).

J. C. Squire is with the Virginia Military Institute, Lexington, VA 24450 USA (e-mail: squirejc@vmi.edu).

J. E. Bodmer is with Kwajalein Range Services, APO, AP 96557 (e-mail: jim.bodmer@gmail.com).

A. B. Moy is with Cellular Engineering Technologies Inc., Coralville, IA 52241 USA (e-mail: abmoy@mac.com).

Color versions of one or more of the figures in this paper are available online at http://ieeexplore.ieee.org.

Digital Object Identifier 10.1109/TBME.2007.893468

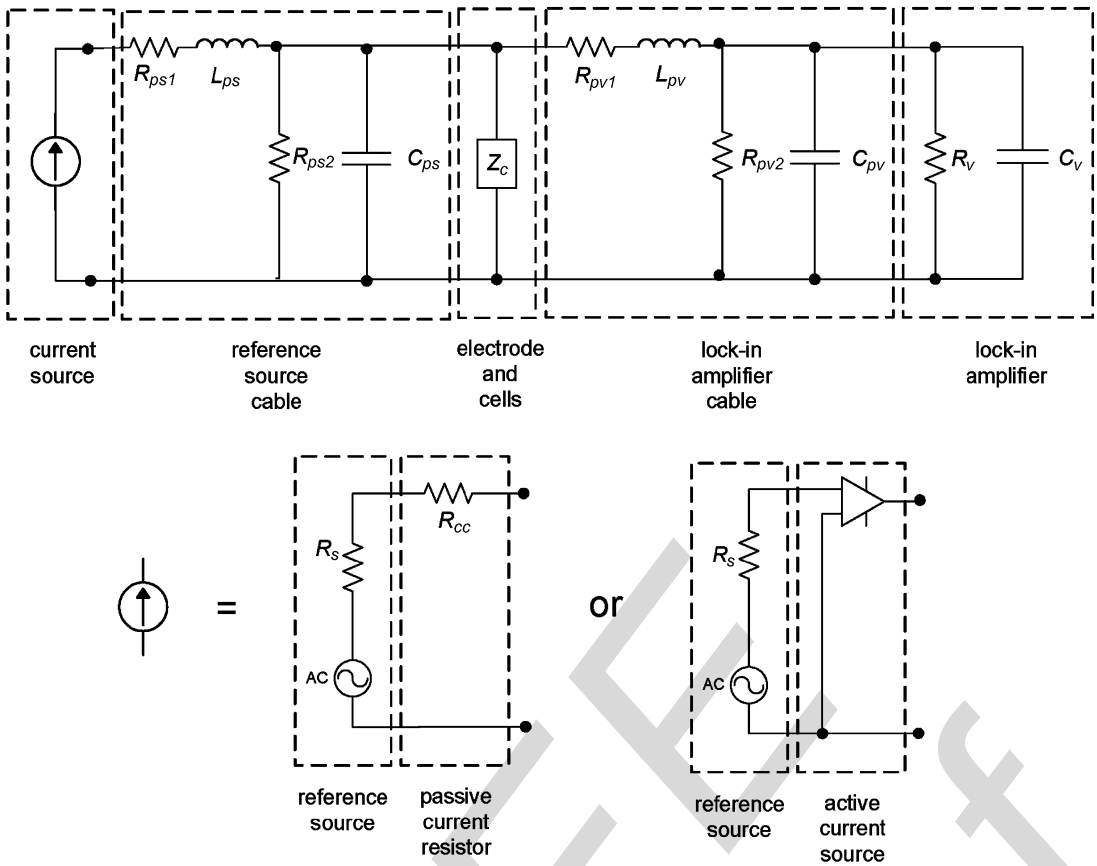

Fig. 1. Cellular impedance biosensor circuit configuration based on a 1-μA current source. In the passive current source, a generator produces a $1\angle 0^\circ \mathrm{V_{pp}}$ voltage via a 50-Ω source resistance, R_s. and a series 1-MΩ resistor, R_{cc} to give an approximately constant $1\angle 0^\circ \mu$A current provided the load is much smaller than R_{cc}. In the active current configuration, a transconductance amplifier provides at least a twenty-five-fold improvement over the passive current source. The lock-in amplifier has an input impedance characterized by the resistance $R_v = 50$ MΩ and capacitance $C_v = 50$ pF the circuit elements, $R_{ps1} = 85$ mΩ, $L_{ps} = 1.5$ μH, $R_{ps2} > 200$ MΩ, and $C_{ps} = 86$ pF represent the reference source coaxial lead series resistance, series inductance, parallel resistive, and parallel capacitive elements, respectively. The circuit elements, $R_{pv1} = 75$ mΩ $L_{pv} = 1.5$ μH $R_{pv2} > 200$ MΩ, and $C_{pv} = 86$ pF represent the corresponding amplifier coaxial lead series and parallel elements.

acids (Sigma). Endothelial cells were inoculated onto a series of gold microelectrodes (Applied Biophysics) coated with fibronectin (BD Biosciences) to facilitate cellular adhesion. Cell covered electrodes were inspected using a Zeiss Axiovert 35 phase contrast microscope to confirm confluence following sixteen hours of attachment in an incubator.

B. Endothelial Cell Voltage Measurements

A lock-in amplifier (Stanford Research SR830) provided a $1\angle 0^\circ \mathrm{V_{pp}}$ ac reference signal with frequencies, $\mathrm{f_L}$, ranging from 10 Hz and 100 kHz to the electrode via either a 1–MΩ resistor or a transconductance amplifier as shown in Fig. 1. In the first configuration, a 1–MΩ resistor, R_{cc}, was used in series with a reference 1 $\mathrm{V_{pp}}$ ac source. The Norton equivalent is a 1-$\mu\mathrm{A_{pp}}$ current source in parallel with a 1–MΩ resistance that delivers approximately 1 $\mu\mathrm{A_{pp}}$ if the absolute value of the input impedance of the rest of the circuit is much less than 1 MΩ. In the second configuration, the voltage controlled current source provided an actively regulated 1-μA current.

The voltage-dependent current source was constructed using a modified Howland current pump with a precision field effect transistor (FET) input high common mode rejection ratio operational amplifier to produce a transimpedance amplifier with an extremely high output impedance [22]. If the resistors are perfectly matched, the output impedance using an AD845 operational amplifier is over 500 MΩ. This degrades at worst to 25 MΩ when using 0.1% resistors but still provides a twenty-five-fold improvement over the passive current source.

The 1-$\mathrm{V_{pp}}$ ac reference generator had a 50-Ω source resistance R_s. The phase sensitive detector input capacitance, C_v, and resistance, R_v, were 10 MΩ and 50 pF, respectively. The coaxial cable connecting the source to the electrode was modeled as a series resistor, R_{ps1}, and inductor, L_{ps}, and a parallel resistor, R_{ps2}, and capacitor, C_{ps}, combination. The lock-in amplifier coaxial cable components R_{pv1}, L_{pv}, R_{pv2}, and C_{pv} were similarly defined. A BK Precision 889A Bench LCR/ESR meter provided direct measurements of the series and parallel coaxial cable impedances. Sensing electrode arrays were purchased from Applied Biophysics. Each array consisted of 5 small 10^{-4} $\mathrm{cm^2}$ gold contacts microfabricated on the bottom of 5 separate wells connected to a single larger 1-$\mathrm{cm^2}$ counter electrode.

The internally generated lock-in reference signal

$$V_L = |V_L| \sin(\omega_L t - \theta_L) \tag{1}$$

where $|V_L|$ is the voltage amplitude, ω_L the frequency, t the time, and θ_L phase, stimulated the electrode circuit and provided a reference waveform during phase sensitive detection. The measured signal was of the form

$$V_S = |V_S|\sin(\omega_S t - \theta_S) \tag{2}$$

where $|V_S|$ is the measured signal amplitude, ω_S the measured signal angular frequency, and θ_S the phase. The lock-in amplifier multiplied the signal and then multiplied it by the lock-in reference using a phase-sensitive detector or multiplier. The output of the phase sensitive detector was the product of two sine waves,

$$V_{\mathrm{PSD}} = |V_S|\sin(\omega_S t - \theta_S) \times |V_L|\sin(\omega_L t - \theta_L). \tag{3}$$

This is equivalent to

$$V_{\mathrm{PSD}} = \frac{1}{2}|V_S||V_L|\cos\left[(\omega_S - \omega_L)t - (\theta_S - \theta_L)\right] - \frac{1}{2}|V_S||V_L|\cos\left[(\omega_S + \omega_L)t - (\theta_S + \theta_L)\right]. \tag{4}$$

The SR830 sampled the electrode voltages using a 16-bit analog-to-digital (A/D) at a rate of 256 kHz and provided a 128 kHz anti-aliasing filter to prevent higher frequency inputs from aliasing below 102 kHz. Digital sampling of this signal was provided at a maximum rate of 512 Hz.

C. Voltage to Impedance Conversion

To find a set of optimal parameters quantifying the cellular barrier function, it is necessary to convert the measured voltages to equivalent impedances based on an instrumental circuit model. Using a series of approximations with increasingly more restrictive assumptions, that are not necessarily justifiable, systematic error propagation into the parameters can be quantified. The following considers both the passive and active current sources shown in Fig. 1.

For the passive current source shown in Fig. 1, the passive reference (PsRef) model can be derived using standard circuit theory [23]

$$Z_c = \frac{V_c Z_{ps1} Z_{ps2}}{Z_{ps2}V_s - V_c\left[\frac{Z_{ps1}Z_{ps2}(Z_{pv2}+Z_v)}{(Z_{pv1}Z_{pv2}+Z_{pv1}Z_v+Z_{pv2}Z_v)} + Z_{ps1} + Z_{ps2}\right]} \tag{5}$$

where V_c is the measured voltage, $Z_{ps1} = R_s + R_{cc} + R_{ps1} + j\omega L_{ps}$, $Z_{ps2} = R_{ps2}/(1+j\omega R_{ps2}C_{ps})$, $Z_{pv1} = R_{pv1} + j\omega L_{pv}$, $Z_{pv2} = R_{pv2}/(1 + j\omega R_{pv2}C_{pv})$, $Z_v = R_v/(1 + j\omega R_v C_v)$, and V_s is the reference voltage source. The term ω represents the angular frequency and $j = \sqrt{-1}$, R_s the reference source impedance, and R_{cc} is a 1-MΩ resistor. The lock-in amplifier has an input impedance characterized by the resistance R_v and capacitance C_v. The circuit elements, R_{ps1}, L_{ps}, R_{ps2}, and C_{ps} represent the reference source coaxial lead series resistance, series inductance, parallel resistance, and parallel capacitance elements, respectively. The circuit elements, R_{pv1}, L_{pv}, R_{pv2}, and C_{pv} represent the corresponding amplifier coaxial lead series and parallel elements. In the limit that the coaxial series components are negligible and the input impedance of the lock-in amplifier is very large, (5) reduces to the passive lead correction (PsLdC) model

$$Z_c = \frac{V_c Z_{ps1} Z_{ps2}}{\left[Z_{ps2}V_s - V_c\left(\frac{Z_{ps1}Z_{ps2}}{Z_{pv2}} + Z_{ps1} + Z_{ps2}\right)\right]}. \tag{6}$$

If the impedance of the coaxial leads is very large then the above relation reduces to the passive voltage divider (PsVD) model

$$Z_c = \frac{V_c Z_{cc}}{(V_s - V_c)}. \tag{7}$$

If the impedance Z_{cc} is much large than Z_c V_s will be much larger than V_c and the above relation will reduce to the passive constant current (PsCC) model

$$Z_c = \frac{Z_{cc}}{V_s}V_c. \tag{8}$$

For the active current source also shown in Fig. 1, basic circuit theory [23] can again be used to derive the active reference (AcRef) model

$$Z_c = \frac{V_c Z_{ps2}}{\left\{Z_{ps2}I_s - V_c\left[\frac{Z_{ps2}(Z_{pv2}+Z_v)}{(Z_{pv1}Z_{pv2}+Z_{pv1}Z_v+Z_{pv2}Z_v)} + 1\right]\right\}} \tag{9}$$

where V_c is the measured electrode voltage, $Z_{ps2} = R_{ps2}/(1 + j\omega R_{ps2}C_{ps})$, $Z_{pv1} = R_{pv1} + j\omega L_{pv}$, $Z_{pv2} = R_{pv2}/(1 + j\omega R_{pv2}C_{pv})$, $Z_v = R_v/(1 + j\omega R_v C_v)$, and I_s is the reference current source. In the limit that the serial impedance components are negligible and the lock in amplifier input impedance is very large (9) reduces to the active lead correction (AcLdC) model

$$Z_c = \frac{V_c Z_{ps2} Z_{pv2}}{[Z_{ps2}Z_{pv2}I_s - V_c(Z_{ps2} + Z_{pv2})]}. \tag{10}$$

In the limit that the coaxial cable impedances are very large, (10) reduces to active constant current (AcCC) model

$$Z_c = \frac{V_c}{I_s}. \tag{11}$$

To illustrate the systematic errors associated with the different circuit approximations, the normalized deviation of the experimentally estimated impedance magnitude and phase are defined as

$$|\Delta Z| = \frac{|Z| - |Z_c|}{|Z_c|} \quad \text{and} \quad \Delta\theta = \theta - \theta_c. \tag{12}$$

The term $|\Delta Z|$ represents the magnitude deviation resulting from the difference in the experimentally estimated impedance magnitude under a given circuit approximation, $|Z|$, and the actual know value $|Z_c|$. The phase deviation, $\Delta\theta$, is given by the difference between the experimentally derived angle, θ and the actual angle, θ_c.

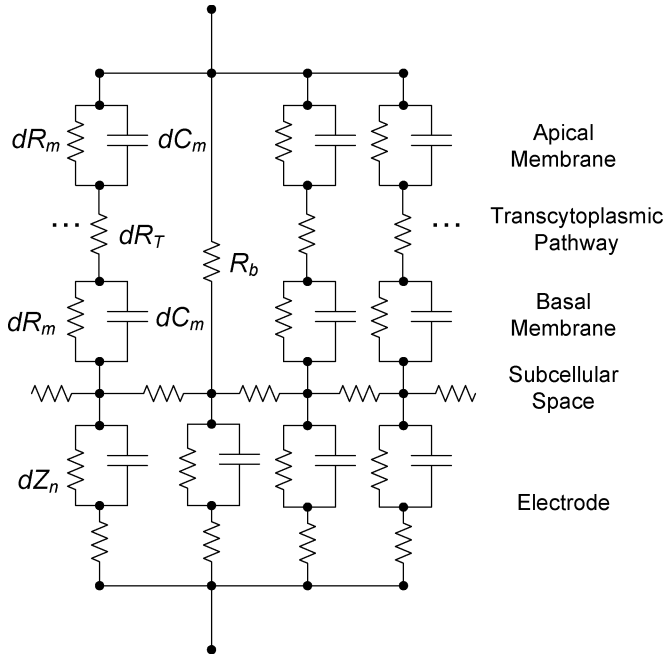

Fig. 2. Cell covered electrode distributed parameter model at a cell-cell junction. A closed form solution for the cell covered impedance Z_c can be derived from this model in terms of bulk cell-cell, cell-matrix, and membrane impedance components. The parameters dR_m, dC_m, dR_T, dZ_n, and R_b represent the distributed membrane resistance, membrane capacitance, transcytoplasmic resistance (assumed zero), naked electrode impedance, and intercellular resistance, respectively.

D. Cellular Impedance Model

Fig. 2 shows the distributed parameter model of the endothelial cell used in this study. The impedance of one membrane is

$$Z_{m1} = \frac{R_m}{1 + j\omega R_m C_m}. \tag{13}$$

where R_m is the membrane resistance and C_m is the membrane capacitance. If the apical and basal membranes are assumed to be identical, the combined impedance of the series combination is

$$Z_m = \frac{2R_m}{1 + j\omega R_m C_m} + R_t. \tag{14}$$

For the purposes of this study, the transcytoplasmic resistance, R_t, is assumed to be negligible. For a cylindrical cell this distributed parameter model is equivalent to the closed from solution [18], [19]

$$\frac{1}{Z_c} = \frac{1}{Z_n}\left[\frac{Z_n}{Z_n + Z_m} + \frac{\frac{Z_m}{Z_n+Z_m}}{\frac{\gamma r_c}{2}\frac{I_0(\gamma r_c)}{I_1(\gamma r_c)} + R_b\left(\frac{1}{Z_n} + \frac{1}{Z_m}\right)}\right] \tag{15}$$

where Z_c is the cell covered impedance, Z_n the naked electrode impedance, Z_m the series combination of the apical and basal membrane impedances, $I_0(\gamma r_c)$ and $I_1(\gamma r_c)$ are modified Bessel functions of the first kind of zero and first order, respectively. The term r_c represents the cell radius and

$$\gamma = \sqrt{\frac{\rho}{h}\left(\frac{1}{Z_n} + \frac{1}{Z_m}\right)} \tag{16}$$

where ρ is the conductivity and h is the separation between the electrode and the cell substratum. The solution depends on R_b, the resistance between the cells per unit area, and α, where

$$\alpha = r_c\sqrt{\frac{\rho}{h}}. \tag{17}$$

Based on this model, electrode polarization effects of the naked electrode [24] are implicitly included in the model by direct experimental measurements. Prior to each electrode inoculation, the naked electrode impedance, Z_n, is measured, the cells are allowed to attach and then the cell covered electrode impedance, Z_c, is measured. As a result, the parameters α, R_b, C_m, and R_m represent the cellular impedance effects and not naked electrode artifacts assuming the attached cells do not change the naked electrode properties.

E. Statistical and Numerical Parameter Optimization

The model to be fitted in this study is of the form

$$Z_c = Z_c(\mathbf{x}; \mathbf{a}) \tag{18}$$

where the measured impedance Z_c has both real, $\Re$, and imaginary, $\Im$, components. The set of independent variables $\mathbf{x}$ in this study consist only of the measured lock-in reference frequency, $\mathrm{f_L}$. The fitting parameter vector, $\mathbf{a}$, has the elements α, R_b, C_m, and R_m. In this experimental system, the noise at different reference frequencies is assumed independent but that the real and imaginary noise components at a given reference frequency can be correlated and have different averages and variances. The reduced chi squared merit function, χ^2_v, in this case is defined as

$$\begin{aligned}\chi^2_v(\alpha, R_b, C_m, R_m) &= \frac{\chi^2(\alpha, R_b, C_m, R_m)}{v} \\ &= \frac{\sum_{k=1}^{N_f}\left[\Re(Z_{ck}-Z_c)\Im(Z_{ck}-Z_c)\right]\Xi_k^{-1}\left[\begin{smallmatrix}\Re(Z_{ck}-Z_c)\\ \Im(Z_{ck}-Z_c)\end{smallmatrix}\right]}{v}\end{aligned} \tag{19}$$

where Ξ_k and Z_{ck} are the covariance matrix and measured impedance at the kth reference frequency and χ^2 is the weighted squared distance between the experimental data and the model function. [25] The term v represents the number of degrees of freedom defined as the number of data points minus the number of free parameters and the term N_f refers to the number of reference frequencies. During a frequency scan noise covariance estimates at each sampled frequency were obtained by sampling the electrode voltages at each frequency at a rate of 512 Hz for 2 s. The electrical noise covariance matrix, Ξ_{ek}, for the k^{th} reference frequency was obtained by repeatedly

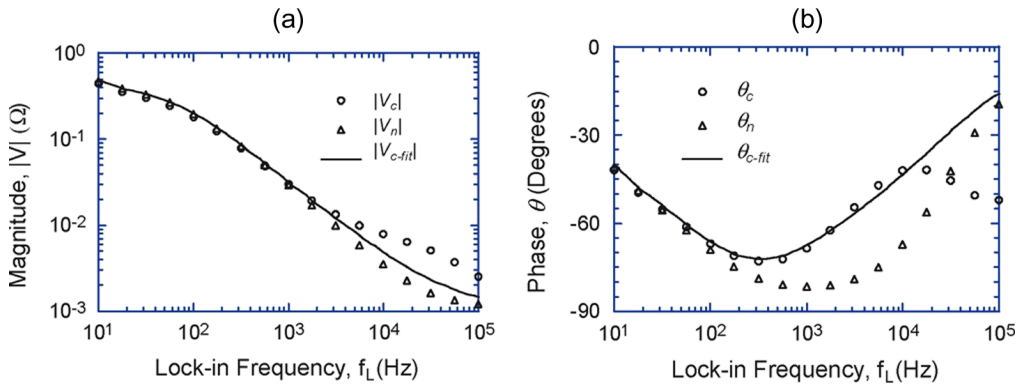

Fig. 3. Magnitude and phase components of the experimentally measured naked and cell covered voltages and a cell covered model fit voltage assuming a constant 1-μA electrode current. (a) The magnitude of the cell covered electrode voltage, $|V_c|$, shows an increase with respected to the naked electrode magnitude, $|V_n|$, but poor agreement with the optimized cell covered voltage fit, $|V_{c-fit}|$. (b) Similarly, the cell covered electrode voltage phase, $|\theta_c|$, is distinctly different from the naked electrode voltage phase, $|\theta_n|$, but is in poor agreement with the model fit voltage phase $|\theta_{c-fit}|$. Each point represents the average of 1024 time sequence voltage measurements sampled at a rate of 512sover 2 s using a 32-ms time constant and 12 dB/decade roll off filter. Error bars representative of the data standard deviation are less than the symbol sizes. The overall quality of the model fit is poor with a reduced chi squared value $\chi^2_v = 3.778 \times 10^6$.

sampling the data at the k^{th} frequency. The real and imaginary values were used to calculate the sample covariance matrix, i.e.,

$$\Xi_{ek} = \begin{bmatrix} S_k^{\Re\Re} & S_k^{\Re\Im} \\ S_k^{\Im\Re} & S_k^{\Im\Im} \end{bmatrix} \tag{20}$$

where

$$S_k^{\Re\Re} = \sum_{i=1}^{N_d} \frac{\Re\left(Z_{ck}^i - \overline{Z}_{ck}\right)\Re\left(Z_{ck}^i - \overline{Z}_{ck}\right)}{(N_d - 1)}$$

$$S_k^{\Re\Im} = \sum_{i=1}^{N_d} \frac{\Re\left(Z_{ck}^i - \overline{Z}_{ck}\right)\Im\left(Z_{ck}^i - \overline{Z}_{ck}\right)}{(N_d - 1)}$$

$$S_k^{\Im\Re} = \sum_{i=1}^{N_d} \frac{\Im\left(Z_{ck}^i - \overline{Z}_{ck}\right)\Re\left(Z_{ck}^i - \overline{Z}_{ck}\right)}{(N_d - 1)}$$

and

$$S_k^{\Im\Im} = \sum_{i=1}^{N} \frac{\Im(Z_{ck} - \overline{Z}_{ck})\Im(Z_{ck} - \overline{Z}_{ck})}{(N_d - 1)}. \tag{21}$$

The averages are calculated from the N_d data samples at each frequency, i.e.,

$$\overline{Z}_{ck} = \frac{1}{N_d}\sum_{i=1}^{N_d} Z_{ck}^i. \tag{22}$$

The A/D contribution to the noise covariance matrix can be estimated as follows. Since the A/D resolution for the SR830 is 16 bits, the A/D interval at the kth frequency can found using the relation

$$\Delta V_{ADk} = \frac{2 \times V_{ks}}{2^{16} - 1} \tag{23}$$

where V_{ks} represents the SR830 amplifier sensitivity setting at the kth frequency. Assuming the A/D noise is uncorrelated, the A/D noise covariance matrix is

$$\Xi_{ADk} = \begin{bmatrix} \frac{(\Delta V_{ADk})^2}{12} & 0 \\ 0 & \frac{(\Delta V_{ADk})^2}{12} \end{bmatrix}. \tag{24}$$

The total system noise variance estimate at the kth frequency is therefore

$$\Xi_k = \Xi_{ek} + \Xi_{ADk}. \tag{25}$$

A total of ten sets of naked and cell covered electrodes were measured and the parameters evaluated. The uncertainty and correlation for a single set of parameters were estimated by using the χ^2 function curvature at its minimum. [26] The biological variability was quantified by evaluating the covariance matrix associated with the 10 sets of parameter measurements. [27]

III. Results

This study can be motivated by attempting to optimize endothelial cell model barrier parameters using electrode voltage measurements converted to equivalent impedances under the assumption of a constant 1-μA electrode current [18]. Fig. 3 shows a representative set of experimentally measured real and imaginary voltages obtained from a naked electrode and the same electrode supporting a confluent endothelial cell monolayer following sixteen hours of attachment. An optimal fit to the cell covered impedance model, Z_c, (15) obtained by minimizing the χ_v^2 function (19), however, produced poor fits with very large χ_v^2 values. The following results identify the random and systematic errors responsible for these poor model fits and the significant improvement in the model fit produced by using filtering and circuit corrections.

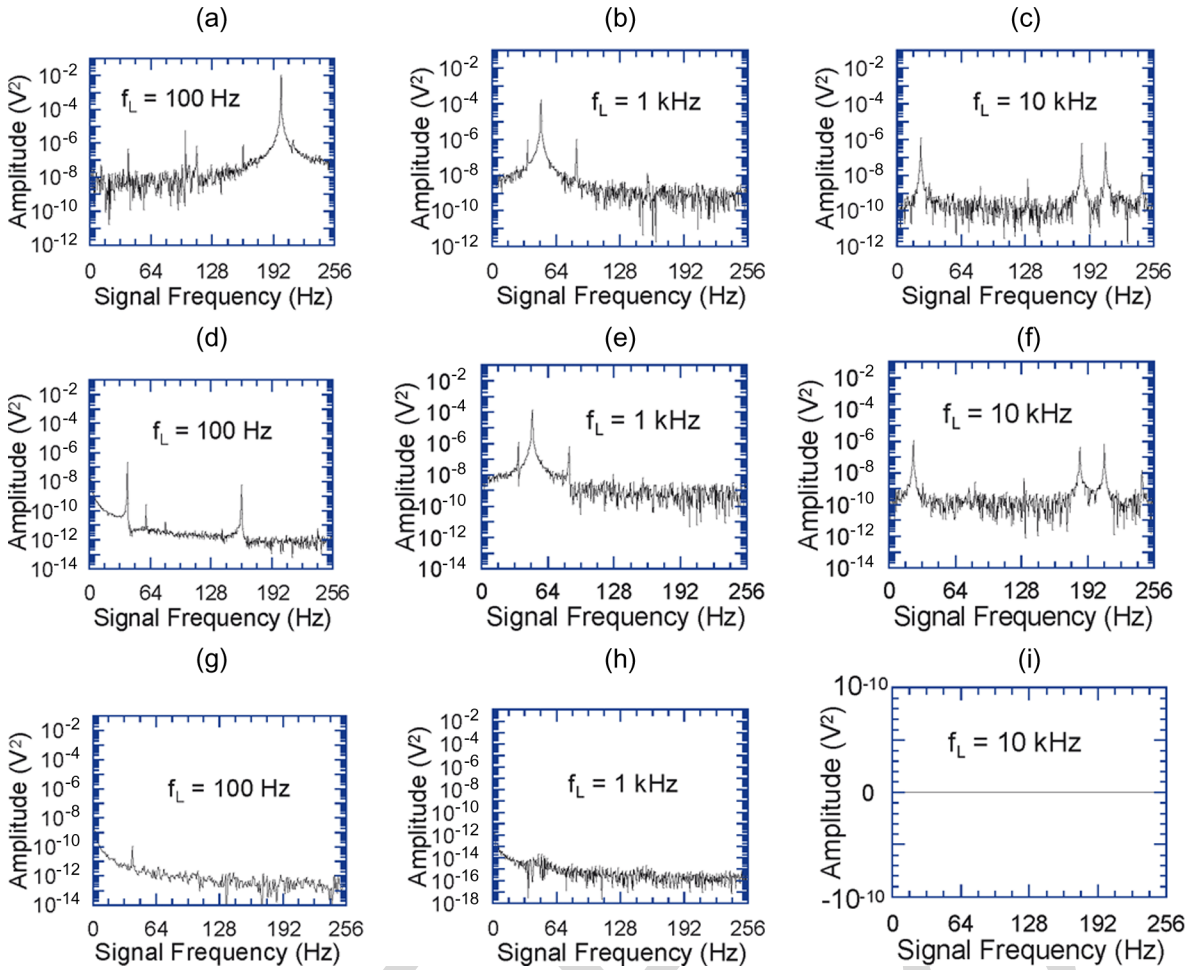

Fig. 4. Power spectral analysis of 1024 experimentally measured in phase naked electrode voltages sampled at a rate of 512 Hz for 2 s. The lock-in amplifier reference frequencies, f_L, were (a), (d) and (g) 100 Hz, (b), (e), and (h) 1 kHz, and (c), (f), and (i) 10 kHz, respectively. (a)–(c) Without synchronization filtering harmonic noise appears at multiples of the reference frequency. (c)—(f) Adding synchronization filtering reveals 60-Hz noise consistent with sum and difference components of the lock-in reference frequency. Additional low-pass filtering with a 30-ms time constant and a 12-dB roll off significantly reduces the 60-Hz noise. (i) At high reference frequencies, the noise level is reduced to the level of the A/D. Aliasing produces spectral folding for signal frequencies exceeding the 256-Hz Nyquist frequency.

A. Random and Deterministic Errors Following Phase Sensitive Detection and Digital Filtering

The different contributions to the instrumental noise can be revealed using a progression of filtering techniques. Beginning with minimal amounts of filtering, synchronous and 60-Hz noise were most clearly observed using a spectral analysis of the acquired voltage data at the different lock-in frequencies. Fluctuations about the measured averages shown in Fig. 3 were smaller than the symbol sizes and produced a consistent pattern of noise. Fig. 4 provides a spectral analysis of 1024 experimentally measured naked electrode voltages sampled at a rate of 512 Hz at the three different lock-in frequencies 100 Hz, 1 kHz and 10 kHz, respectively, under different filter settings. The top row of Fig. 4 shows the spectra obtained with a low pass filter time constant of 10 μs and a 6 dB/decade roll-off. Adding synchronous filtering produced the middle row and increasing the filter time constant to 30 ms and the roll off to 12 dB/decade produced the bottom row. Without synchronous filtering, a 100-Hz reference frequency produced large artifacts at multiples of the lock-in reference frequency. At 1 and 10 kHz reference frequencies, artifacts consistent with the spectral folding of the reference frequency harmonics or 60-Hz noise were present. At low reference frequencies, synchronous filtering significantly reduced the harmonic noise components but revealed artifacts consistent with 60-Hz noise. The 100-Hz reference frequency spectrum contained sum and difference 60-Hz noise components at 40 and 160 Hz, respectively. The bottom row of three spectra in Fig. 4 demonstrates that a filter with a 30-ms time constant and 12 dB/decade roll off effectively removed most of the synchronous and white Gaussian instrumental noise. At higher reference frequencies the filtering reduced the noise to the level of the A/D and the standard deviation of these measurements went to zero.

The effect of filtering on statistical measures of the time domain fluctuations gives a complementary perspective to the frequency analysis. Using these statistics in a Monte Carlo simulation also provides a link to the parameter errors for a given level of filtering. Fig. 5 provides a statistical summary ofexperimentally acquired naked electrode voltage fluctuations and their propagation into parameter error estimates under different filter settings. The top two rows of figures show the square root of the noise covariance matrix determinant associated with 1024 data points sampled at a rate of 512 Hz at each reference frequency

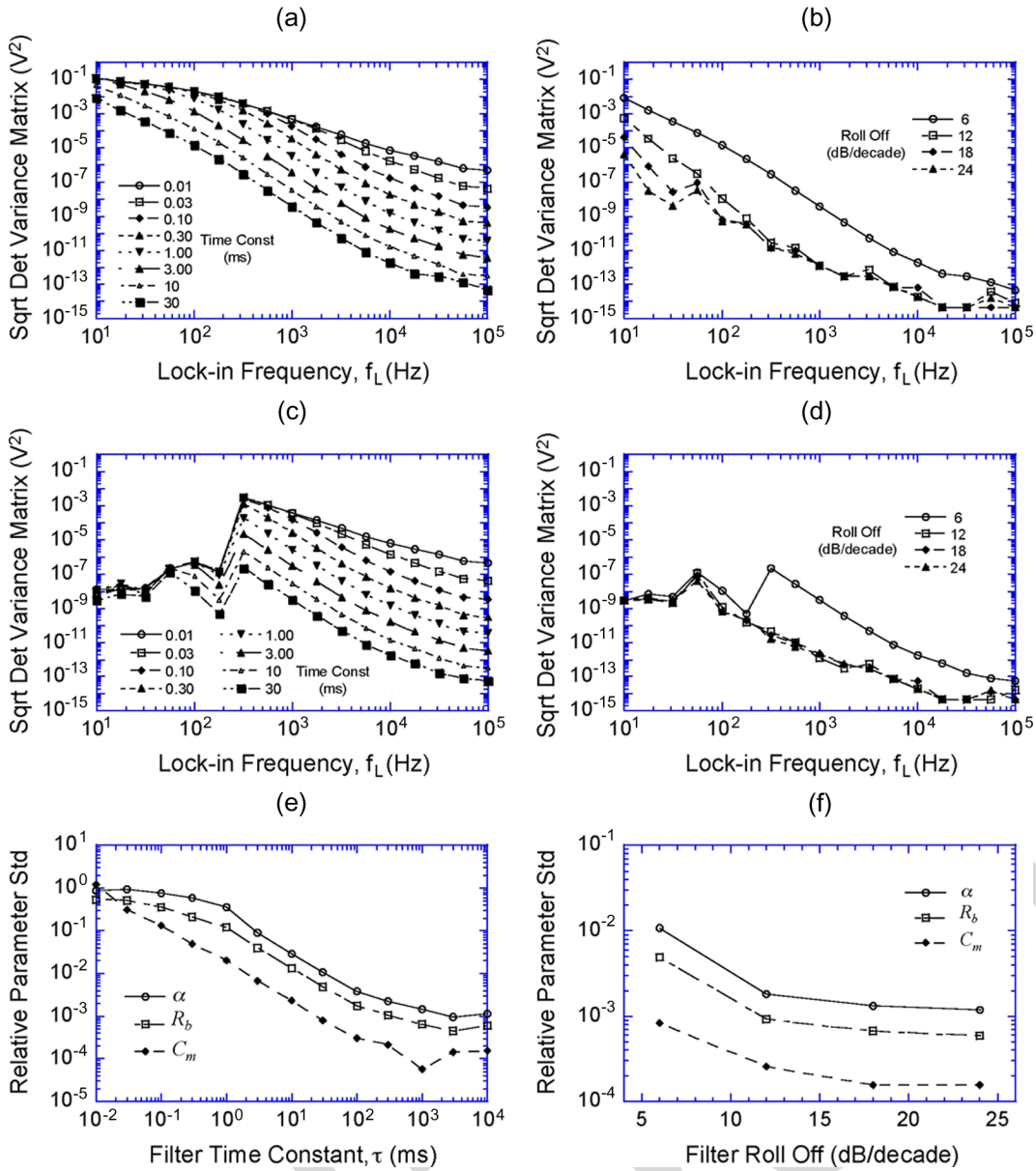

Fig. 5. Experimentally acquired naked electrode voltage statistical summary and noise propagation into parameter error estimates under different filter settings. (a), (c), and (e) Effects of increasing filter time constant with a 6 dB/decade roll off are shown while (b), (d), and (f) illustrate the effects of increasing filter roll off with a fixed filter time constant of 30 ms. (c) and (d) Represent the same experiment illustrated in (a) and (b), but with the addition of synchronization filtering. The parameter error fluctuations, shown in (e) and (f), were evaluated using Monte Carlo simulations based on the measured naked electrode statistics.

with changes in filter time constant and roll off. The left column of figures illustrates the effect of increasing the filter time constant while holding the roll off constant at 6 dB/decade. The right column of figures shows the effects of increasing the filter roll off while holding the filter time constant at 30 ms. The variance estimates include the A/D error based on (25). For a given filter setting, the instrumental noise variance decreases with increasing lock-in reference frequency. The middle row of plots illustrates the effects of including synchronous filtering below 200 Hz. The bottom row of figures show the corresponding parameter estimates obtained from these voltage measurements after scaling them by a factor of 10^6, assuming a constant 1-μA electrode current. Based on Monte Carlo simulations using the naked electrode noise statistics determined for each filter setting, the parameter fluctuations show a monotonic decrease with increasing filtering.

B. Systematic Error Sources and Correction

With reference to Fig. 1, the measured coaxial circuit model parameters for the source and voltage cables using the BK Precision 889A Bench LCR/ESR meter were as follows. The source coaxial cable components had the values: $R_{ps1} = 85$ mΩ, $L_{ps} = 1.5$ μH, $R_{ps2} > 200$ MΩ, and $C_{ps} = 86$ pF. The lock-in amplifier coaxial cable components had the values: $R_{pv1} = 75$ mΩ, $L_{pv} = 1.5$ μH, $R_{pv2} > 200$ MΩ, and $C_{pv} = 86$ pF. Changes in these parameters were negligible over the lock-in amplifier reference frequency range used in this study. Additional capacitances associated with the switch and connections were also observed and included in the following analysis.

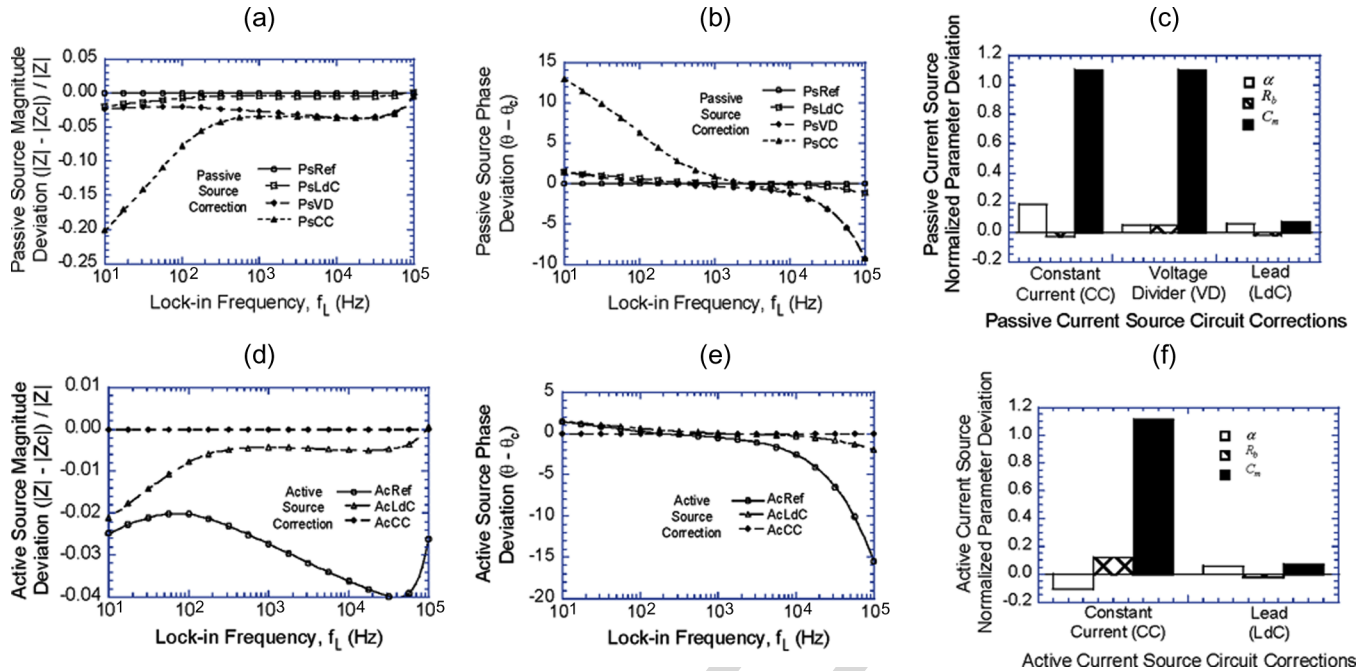

Fig. 6. Passive and active current model systematic error propagation. (a) The passive source impedance magnitude deviations, (b) impedance phase deviations and (c) parameter estimates associated with the constant current, PsCC, voltage divider, PsVD, and lead correction, PsLdC, show increasing agreement with the reference model, PsRef. (d) The corresponding active source impedance magnitude deviations, (e) impedance phase deviations, and (f) parameter errors associated with the constant current, AcCC, voltage divider, AcVD, and lead correction AcLdC models show a similar increase in agreement with the reference state AcRef. Passive and active constant current (PsCC and AcCC) models produce the largest systematic errors. Although a passive voltage divider (PsVD) correction improves the passive current source impedance estimates, lead correction models (PsLdC and AcLdC) are required to reduce the impedance and parameter systematic errors compared to the reference models (PsRef and AcRef).

Fig. 6 shows the propagation of systematic errors produced by the voltage to impedance conversion method into the impedance magnitude, impedance phase and cellular barrier function parameter values for a cell covered electrode. The PsCC model (8) produced systematic errors at both low and high frequency impedance estimates and large systematic errors in the membrane capacitance. The PsVD model (7) corrected the low frequency systematic errors produced by the electrode voltage divider effect but failed to correct the higher systematic errors produced by circuit capacitances. Although the active current source overcame systematic errors associated by low frequency electrode impedance voltage divider effects, it still failed to correct the parameter errors produced by circuit capacitive elements. A lead correction model for both passive, PsLdC (6), and active, AcLdC (10), current sources corrected the high frequency systematic errors produced by the circuit capacitances.

Fig. 7 summarizes the propagation of lead capacitances into the estimated impedance and parameter deviations under the assumption of a constant current voltage to impedance conversion. In addition to the low frequency deviations produced by electrode voltage divider effect, Fig. 7 shows that at frequencies in excess of 5.6 kHz the estimated impedance and parameter deviations are increasingly sensitive functions of the circuit capacitances. The active current source corrects circuit voltage divider effects but does not compensate for circuit capacitances. The parameter deviations produced by passive and active current source regulation with increasing coaxial lead capacitances show very similar patterns.

C. Corrections and Biological Summary

Fig. 8 shows the same voltage measurements shown in Fig. 3 filtered and converted to equivalent impedances with corrections for circuit capacitive elements and voltage divider effects effects using (5). Compared to the analysis shown in Fig. 3, the reduced chi squared, χ_v^2 given by (19), was reduced from 3.778×10^6 to 6.682×10^4 indicating a significant improvement in the optimization. For this representative set of experimental measurements, the optimized parameters were $\alpha = 7.310 \pm 0.002\ \Omega^{0.5} \cdot \mathrm{cm}$, $R_b = 2.840 \pm 0.004\ \Omega \cdot \mathrm{cm}^2$, $C_m = 0.4638 \pm 0.00003\ \mu\mathrm{F} \cdot \mathrm{cm}^{-2}$, and $R_m = 9 \pm 3\ \mathrm{k}\Omega \cdot \mathrm{cm}^2$. The correlation coefficients were $\alpha - R_b = -0.9625$, $\alpha - C_m = -0.8160$, $\alpha - R_m = -0.8269$, $R_b - C_m = 0.9019$, $R_b - R_m = 0.8807$, and $C_m - R_m = 0.8507$. Note that the error estimates and correlation coefficients in this representative case were estimated by calculating the curvature of the χ^2 at the optimized minimum. [26] The numerical parameter error estimates and the correlation coefficients between the four parameters α, R_b, C_m, and R_m, obtained in this manner showed a consistent pattern over the ten different samples measured in this study. The parameter α was consistently negatively correlated with R_b, C_m and R_m. The parameter R_b was consistently positively correlated with C_m and R_m and the parameter C_m was always positively correlated with R_m. This raises issues related to the identifiability of these parameters. Small changes in one parameter can be easily compensated for by changes in one or more of the other parameters to give the same quality of the fit. In this study, estimates of the fourth parameter, R_m, consistently had large errors associated with it based on the χ^2 curvature.

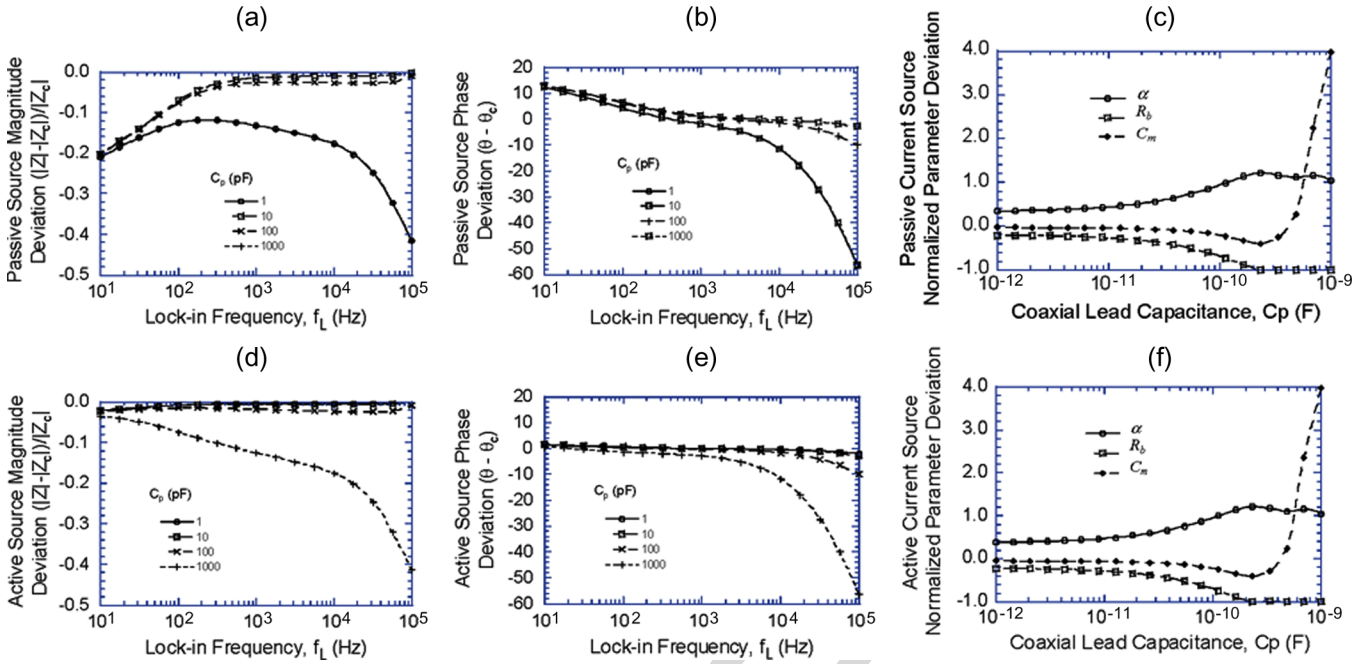

Fig. 7. (a)–(c) Impedance magnitude and phase sensitivity analysis for coaxial cable capacitances using passive and (d)–(f) active current sources. Increasing coaxial cable capacitances produce increasing parameter errors. The membrane capacitance parameter, C_m, is very susceptible to this artifact. Changing C_{ps} and C_{pv} produces similar effects. The true values of α, R_b, C_m and R_m are $2\ \Omega^{0.5}\cdot$cm, $2\ \Omega\cdot\text{cm}^2$, $2\ \mu\text{F}\cdot\text{cm}^{-2}$, and $10\ \text{k}\Omega\cdot\text{cm}^2$, respectively. The similarity of the last column of figures indicates that the active current source does not correct the parameter systemic errors produced by circuit capacitances.

Compared to individual parameter error estimates, the biological variability among the ten sets of parameters in this study were much greater and the correlation between the parameters much less. The statistics of the ten confluent endothelial cell impedance parameter estimates gave the following averages and standard deviations: $\alpha = 7 \pm 2\ \Omega^{0.5}\cdot\text{cm}$, $R_b = 7 \pm 3\ \Omega\cdot\text{cm}^2$, $C_m = 0.5 \pm 0.2\ \mu\text{F}\cdot\text{cm}^{-2}$, and $R_m = 5 \pm 3\ \Omega\cdot\text{cm}^2$. The correlation coefficients were $\alpha - R_b = -0.0499$, $\alpha - C_m = -0.6163$, $\alpha - R_m = 0.4178$, $R_b - C_m = -0.4392$, $R_b - R_m = -0.0883$, and $C_m - R_m = -0.5047$. The biological variability evaluated using standard statistical methods [25] was therefore significantly greater than parameter error estimates obtained from a single optimization. [26]

IV. Discussion

The accuracy and precision of cellular barrier function parameters are complicated functions of the data acquisition and analysis. The few studies that have examined these model parameter estimation methods for this application, however, do not consider instrumental noise. [21] Voltage measurements obtained from a gold two-electrode configuration using phase sensitive detection, however, are corrupted by harmonic, 60 Hz, white Gaussian, and quantization errors. In addition, the voltage to impedance conversion introduces systematic errors depending on the underlying instrument circuit assumptions. Model parameter stability and the numerical methods introduce additional errors. Systematically identifying and reducing each of these errors is, therefore, an important consideration in quantitative cellular barrier function parameter estimation.

Although phase sensitive detection can be used to recover small signals, this technique can potentially introduce a number of artifacts into the data. [28] The phase sensitive detector output consists of two ac signals, one at the difference frequency $(\omega_S - \omega_L)$ and the other at the sum frequency $(\omega_S + \omega_L)$. If the reference frequency ω_L equals the signal frequency ω_S, the difference frequency component will be a DC signal. In this case, the filtered phase sensitive detector output will be

$$V_{PSD} = \frac{1}{2}|V_S||V_L|\cos(\theta_S - \theta_L) \tag{26}$$

where $|V_S|$ is the signal voltage amplitude, $|V_L|$ the lock-in reference voltage amplitude, θ_S the signal voltage phase, and θ_L the lock-in reference phase. The output signal is therefore a DC signal proportional to the signal amplitude. The sum frequency, however, introduces a second reference frequency harmonic. In addition, noise signals that appear at frequencies other than the reference frequency appear as sum and difference signals of the reference and noise frequencies. Without synchronous filtering, harmonic noise was a significant noise source below 200 Hz. Using synchronous filtering, however, revealed sum and difference 60-Hz noise components. Depending on the reference frequency, sampling rate, and possible aliasing effects, these noise components can appear at frequencies that can be easily misinterpreted as biological effects.

The very large change in the noise variance as a function of frequency, shown in Fig. 5, has important consequences for the numerical analysis of this type of data. In a least squares based non-linear fitting algorithm it is important to weight the data less if it has a higher variance. [25] Weighting the data equally in this case would put too much emphasis on the lower frequency data points that have relatively high amounts of noise. Introducing the measured noise estimate into the optimization overcomes this problem. At higher frequencies where the filtering effectively reduces the noise level to the A/D level it is important to

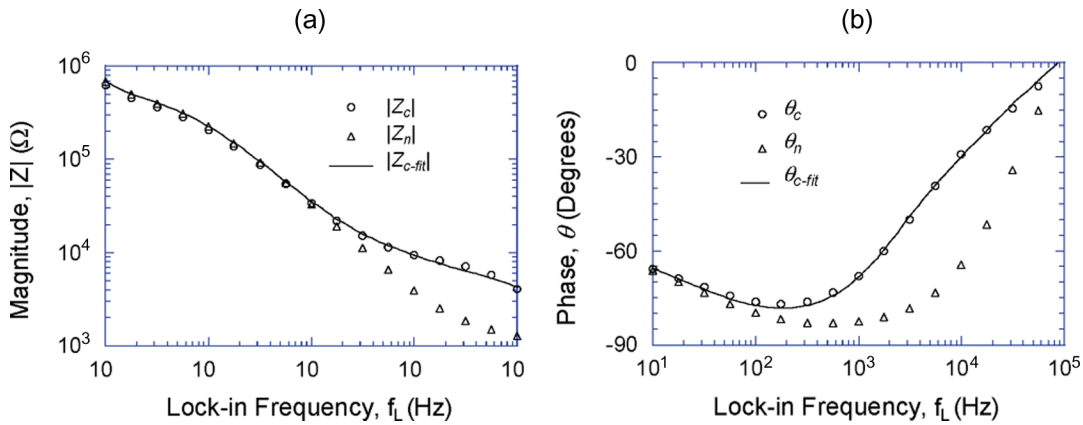

Fig. 8. Naked and cell covered impedance estimates from experimental measurements and an optimal fit to the cell covered impedance following filtering and circuit corrections. (a) Filtering and circuit corrections provide a more accurate estimate of the naked electrode impedance magnitude, $|Z_n|$, and cell covered electrode impedance magnitude, $|Z_c|$, and improves the numerical fit to the cell covered electrode $|Z_{c-fit}|$. (b) Filtering and circuit corrections also improve the accuracy of the naked electrode impedance phase, $|\theta_n|$, and cell covered electrode phase, $|\theta_c|$, and improves the numerical fit to the cell covered electrode $|\theta_{c-fit}|$. The optimized fitted parameter values to the cell covered electrode measurement in this case are: $\alpha = 5.07 \pm 0.04$, $R_b = 6.77 \pm 0.04$, $C_m = 5.130 \pm 0.006$, and $R_m = 2.2 \pm 0.8$. The correlation coefficients are $\alpha - R_b = -0.9992$, $\alpha - C_m = -0.9622$, $\alpha - R_m = -0.4477$, $R_b - C_m = 0.9709$, $R_b - R_m = 0.8714$, and $C_m - R_m = 0.8108$. The statistics for a single measurement were obtained from the curvature of the χ_v^2 minimum. The reduced chi squared value is $\chi_v^2 = 6.682 \times 10^4$.

include A/D noise estimates into the algorithm to avoid singularities in the optimization.

The electrode voltage to impedances conversion can potentially introduce a number of frequency dependent systematic errors. Impedance estimates in this type of cellular microsensor have traditionally been made assuming that the current provided by a 1-V source across a 1-MΩ resistor in series with the electrode is a constant 1 μA. [1]–[3], [18].With such a passive current source, however, electrode loading produces a voltage divider effect that leads to frequency dependent systematic errors in the estimated impedance if a constant current assumption is made. For a gold electrode this is particularly a problem at low frequencies where the electrode impedance is relatively large compared to the 1-MΩ resistor. Introducing an active current source to maintain a constant 1-μA current corrects these low frequency voltage divider effects. Both the passive and the active current sources, however, suffer from artifacts at higher frequencies where circuit capacitances produce systematic errors in the estimated electrode impedance.

In both the passive and the active current source circuit configurations analytical formula can be used to convert the measured voltages into equivalent impedances based on different circuit approximations. This has the potential to reduce systematic errors associated with voltage divider effects and capacitive impedance elements not accounted for in a constant current assumption. [17] The resulting transformed noise that enters the numerical optimization, however, can contribute to additional parameter instability depending on the underlying numerical methods. In this case, Monte Carlo simulations using the transformed noise should be used to quantify the parameter errors. [26]

The coaxial cables introduce capacitive elements into the circuit that should be minimized by using either short cable lengths or calibration standards. The measured series resistive and inductive components, however, were found to be negligible as expected. In addition, the large resistance between the cable inner conductor and outer sheath was large enough to discount. The parallel capacitance introduced by the coaxial cable produced systematic errors at higher frequencies. As a result, parameter estimates sensitive to higher frequency impedances will be most susceptible.

Including filtering and corrections for capacitive circuit elements increased the quality of the fit significantly from $\chi_v = 3.778 \times 10^6$ to $\chi_v = 6.682 \times 10^4$ for the representative case shown in Figs. 3 and 8. Similar improvements were observed for the remaining nine samples considered in this study. The reduced chi squared value should, however, be on the order of unity. The fact that is much higher than this, even after filtering and systematic error correction, indicates that other sources of error exist. The model itself, for example, may not be appropriate. Other effects such as instrumental and biological drift or numerical instabilities may also be contributing to the large reduced chi squared values.

REFERENCES

[1] I. Giaever and C. R. Keese, "Monitoring fibroblast behavior in tissue culture with an applied electric field," *Proc. Nat. Acad. Sci. USA*, vol. 81, pp. 3761–3764, 1984.

[2] ——, "Use of electric fields to monitor the dynamical aspect of cell behavior in tissue culture," *IEEE Trans. Biomed. Eng.*, vol. BME-33, pp. 242–247, 1986.

[3] C. R. Keese and I. Giaever, "A biosensor that monitors cell morphology with electrical fields," *IEEE Eng. Med. Biol.*, vol. 13, no. 3, pp. 402–408, Jun.-Jul. 1994.

[4] C. A. Ellis, C. Tiruppathi, R. Sandoval, W. D. Niles, and A. B. Malik, "Time course of recovery of endothelial cell surface thrombin receptor (par-1) expression," *Am. J. Physiol. (Cell Physiol.)*, vol. 276, pp. C38–C45, 1999.

[5] N. Kataoka, K. Iwaki, K. Hashimoto, S. Mochizuki, Y. Ogasawara, M. Sato, K. Tsujioka, and F. Kajiya, "Measurements of endothelial cell-to-cell and cell-to-substrate gaps and micromechanical properties of endothelial cells during monocyte adhesion," *Proc. Nat. Acad. Sci.*, vol. 99, pp. 15638–15643, 2002.

[6] H. Lum, Z. Hao, D. Gayle, P. Kumar, C. E. Patterson, and M. D. Uhler, "Vascular endothelial cells express isoforms of protein kinase a inhibitor," *Am. J. Physiol. Cell Physiol.*, vol. 282, pp. C59–C66, 2002.

[7] A. B. Moy, K. Blackwell, N. Wang, K. Haxhinasto, M. K. Kasiske, J. Bodmer, G. Reyes, and A. English, "Phorbol ester-mediated pulmonary artery endothelial barrier dysfunction through regulation of actin cytoskeletal mechanics," *Am. J. Physiol. Lung Cell Mol. Physiol.*, vol. 287, pp. L153–L167, 2004.

[8] A. B. Moy, B. Scott, S. Shasby, and D. M. Shasby, "The effect of histamine and cyclic adenosine monophosphate on myosin light chain phophorlylation in human umbilical vein endothelial cells," *J. Clin. Invest.*, vol. 92, pp. 1198–1206, 1993.
[9] A. B. Moy, J. VanEngelenhoven, J. Bodmer, J. Kamath, C. Keese, I. Giaver, S. Shasby, and D. M. Shasby, "Histamine and thrombin modulate endothelial focal adhesion through centripetal and centrifugal forces," *J. Clin. Invest.*, vol. 97, pp. 1020–1027, 1996.
[10] A. B. Moy, M. Winter, A. Kamath, K. Blackwell, G. Reyes, I. Giaever, C. Keese, and D. M. Shasby, "Histamine alters endothelial barrier function at cell-cell and cell-matrix sites," *Am. J. Physiol. Lung. Cell Mol. Physiol.*, vol. 278, pp. L888–L898, 2000.
[11] V. NandaKumar, A. E. English, A. B. Moy, M. Mahfouz, R. Ward, K. Kruse, S. Kirkpatrick, and M. H. Goldman, "Real time monitoring of endothelial cell actin filament disruption by cytochalasin d using a cellular impedance biosensor," presented at the 2nd IEEE-EMBS Int. Summer School Symp. Medical Devices and Biosensors (ISSS-MDBS), 2004, Hong Kong.
[12] E. Noiri, E. Lee, J. Testa, J. Quigley, D. Colflesh, C. R. Keese, I. Giaever, and M. S. Goligorsky, "Podokinesis in endothelial cell migration: Role of nitric oxide," *Am. J. Physiol.*, vol. 274, pp. C236–C244, 1998.
[13] J. E. Phelps and N. DePaola, "Spatial variations in endothelial barrier function in disturbed flows in vitro," *Am. J. Physiol. Heart Circ. Physiol.*, vol. 278, pp. H469–H476, 2000.
[14] R. Sandoval, A. B. Malik, R. D. Minshall, P. Kouklis, C. A. Ellis, and A. Tiruppathi, "Ca2+ signalling and pkca activate increased endothelial permeability by disassembly of ve-cadherin junctions," *J. Physiol.*, vol. 533, pp. 433–445, 2001.
[15] C. Tiruppathi, A. B. Malik, P. J. D. Vecchio, C. R. Keese, and I. Giaever, "Electrical method for detection of endothelial cell shape change in real time: Assessment of endothelial barrier function," *Proc. Nat. Acad. Sci. USA*, vol. 89, pp. 7919–7923, 1992.
[16] J. Wegener, C. R. Keese, and I. Giaever, "Electric cell-substrate impedance sensing (ecis) as a noninvasive means to monitor the kinetics of cell spreading to artificial surfaces," *Exp. Cell Res.*, vol. 259, pp. 158–166, 2000.
[17] C. Xiao, B. Lachance, G. Sunahara, and J. H. T. Luong, "An in-depth analysis of electric cell-substrate impedance sensing to study the attachment and spreading of mammalian cells," *Anal. Chem.*, vol. 74, pp. 1333–1339, 2002.
[18] I. Giaever and C. R. Keese, "Micromotion of mammalian cells measured electrically," *Proc. Nat. Acad. Sci. USA*, vol. 88, pp. 7896–7900, 1991.
[19] ——, "Correction: Micromotion of mammalian cells measured electrically," *Proc. Natl. Acad. Sci. USA*, vol. 90, p. 1634, 1993.
[20] C.-M. Lo, C. R. Keese, and I. Giaever, "Impedance analysis of mdck cells measured by electric cell-substrate impedance sensing," *Biophys. J.*, vol. 69, pp. 2800–2807, 1995.
[21] J. E. Bodmer, A. English, M. Brady, K. Blackwell, K. Haxinasto, S. Fotedar, K. Borgman, E.-W. Bai, and A. B. Moy, "Modeling error and stability of endothelial cytoskeletal-membrane parameters based on numerical modeling transendothelial impedance as resistor and capacitor in series," *Am. J. Phys.*, vol. 289, pp. C735–C747, 2005.
[22] P. Horowitz and W. Hill, *The Art of Electronics*, 2nd ed. Cambridge, U.K.: Cambridge Univ. Press, 1989.
[23] D. J. Irwin and Chwan-Hwa, *Basic Engineering Circuit Analysis*. New York: , 1990.
[24] L. A. Geddes, "Historical evolution of circuit models for the electrode-electrolyte interface," *Ann. Biomed. Eng.*, vol. 25, pp. 1–14, 1997.
[25] P. R. Bevington, *Data Reduction and Error Analysis for the Physical Sciences*. New York: McGraw-Hill, 1969.
[26] W. H. Press, W. T. Bettering, S. A. Teukolsky, and B. P. Flannery, *Numerical Recipes in c++ the Art of Scientific Computing*, 2nd ed. Cambridge, U.K.: Cambridge Univ. Press, 2002.
[27] R. A. Johnson and D. W. Wichern, *Applied Multivariate Statistical Analysis*. Upper Saddle River, NJ: Prentice-Hall, 1982.
[28] M. L. Meade, *Lock-In Amplifiers: Principles and Applications*, ser. Iee electrical measurement series. London, U.K.: Peter Peregrinus/IEE, 1983.

Anthony E. English received the B.A.Sc degree in engineering physics from Simon Fraser University, Burnaby, BC, Canada, in 1986, the M.A.Sc. degree in electrical and biomedical engineering from the University of Toronto, Toronto, ON, Canada, in 1989, and the Ph.D. degree in medical engineering and medical physics from the Harvard-MIT division of Health Sciences and Technology, Cambridge, MA, in 1996.

He has held research positions at the TRIUMF Meson research facility, Vancouver, BC, Canada, Bell Northern Research in Ottawa, ON, Canada, and Sony Corporation, Atsugi, Japan. He joined the faculty at the University of Tennessee , Knoxville, in 2002 where he teaches senior and graduate courses in biotransport, tissue engineering, and cellular dynamics. His interests include the application of non-linear control theory and stochastic geometry to soft biomaterial phase transitions and cellular level phenomena.

Prof. English is the recipient of a National Science Foundation CAREER Award and while at MIT received a Raytheon Fellowship and a Rhône-Poulenc Rorer Fellowship.

James C. Squire (M'86-SM'04) received the B.Sc. degree in electrical engineering from West Point, West Point, NY, in 1989, the M.Sc. degree in electrical engineering and computer science from the Massachusetts Institute of Technology (MIT), Cambridge, in 1996, and the Ph.D. degree in electrical engineering and computer science from MIT in 2000.

He served in the Gulf War as a Military Intelligence Officer. While at MIT, he taught, consulted in patent litigation and engineering, and performed biomedical engineering research. He joined the Virginia Military Institute (VMI) Department of Electrical and Computer Engineering (ECE) faculty in 2000 where he is currently an Associate Professor. He teaches sophomore through senior-level courses in circuits, linear signals and systems, digital signal processing, senior seminar, and supervises independent research and honors projects. His interests are in engineering pedagogy, instrumentation, patent law, mechatronics, and biomedical engineering.

Prof. Squire is a member of the American Society of Engineering Educators and the National Society of Professional Engineers. He was also the recipient of a Bronze Star while serving in the Gulf War and was selected as Virginia's outstanding junior faculty member in 2004 by the Virginia Council of Higher Education.

James E. Bodmer received the B.Sc. degree in biomedical engineering in 1997 and the M.Sc. degree in 2003 in electrical and computer engineering from the University of Iowa, Iowa City.

He has worked as an Engineer at Rockwell International, Cedar Rapids, IA, on global positioning systems and DynCorp on remote telemetry tracking. He has worked extensively with various agencies that include the Defense Advanced Research Projects Agency (DARPA), U.S. Army Research Laboratory (ARL), Naval Research Laboratory, Office of Aviation Research (AAR), as well as many other government and industry research funding partners. He currently serves in the U.S. Marine Corps and works for Kwajalein Range Services as a digital hardware engineering on radar sensors located in the Marshall Islands. His research and professional interests include biosystems mathematical modeling, signal processing, and artificial intelligence.

Alan B. Moy received the B.Sc. degree in biochemistry from the University of California, Davis, in 1981 and the M.D. degree from Creighton University , Omaha, NE, in 1985.

He completed a residency in Internal Medicine at St. Louis University, St. Louis, MO, in 1988. After completing a fellowship in Pulmonary and Critical Care Medicine at the University of Iowa in 1993, he served as a Faculty Member in the Department of Internal Medicine and Biomedical Engineering. He is currently the President of Cellular Engineering Technologies in Coralville, IA. His basic and applied research interests involve the application of molecular biology, gene therapy, advanced image processing methods, biomaterials, micro-biomechanical approaches, microfabrication technologies, and microimpedance techniques for evaluating complex cellular physiological processes and developing gene therapies to treat acute lung injury.

Dr. Moy is a member of the American Thoracic Society, the American Heart Association, and the American College of Chest Physicians.